Nanoscale Research Letters
a SpringerOpen Journal

NANO EXPRESS   **Open Access**

Modification of crystal anisotropy and enhancement of magnetic moment of Co-doped SnO$_2$ thin films annealed under magnetic field

Sagrario M Loya-Mancilla[1], Pankaj Poddar[2], Raja Das[2], Hilda E Esparza Ponce[1], Ivan L Templeton-Olivares[1], Oscar O Solis-Canto[1], Carlos E Ornelas-Gutierrez[1], Francisco Espinosa-Magaña[1] and Sion F Olive-Méndez[1*]

Abstract

Co-doped SnO$_2$ thin films were grown by sputtering technique on SiO$_2$/Si(001) substrates at room temperature, and then, thermal treatments with and without an applied magnetic field (H$_{TT}$) were performed in vacuum at 600°C for 20 min. H$_{TT}$ was applied parallel and perpendicular to the substrate surface. Magnetic M(H) measurements reveal the coexistence of a strong antiferromagnetic (AFM) signal and a ferromagnetic (FM) component. The AFM component has a Néel temperature higher than room temperature, the spin axis lies parallel to the substrate surface, and the highest magnetic moment $m = 7$ μ$_B$/Co at. is obtained when H$_{TT}$ is applied parallel to the substrate surface. Our results show an enhancement of FM moment per Co^{+2} from 0.06 to 0.42 μ$_B$/Co at. for the sample on which H$_{TT}$ was applied perpendicular to the surface. The FM order is attributed to the coupling of Co^{+2} ions through electrons trapped at the site of oxygen vacancies, as described by the bound magnetic polaron model. Our results suggest that FM order is aligned along [101] direction of Co-doped SnO$_2$ nanocrystals, which is proposed to be the easy magnetization axis.

Keywords: Crystal anisotropy; Magnetic anisotropy; Thin film; Ferromagnetism; Antiferromagnetism; Magnetic moment; Spin axis; Diluted magnetic oxide

Background

Research in semiconducting oxide thin films has fundamental importance due to its wide range of applications in optoelectronics [1], photoluminescence [2], sensing devices [3], etc. Furthermore, experiments with nanomaterials where the electron charge and its spin orientation, regarded as an additional degree of freedom, are together considered to produce new physical effects situated on the field of spintronics, which is a wide research area that offers options to fabricate faster and lower energy consuming solid state devices. In this field, one of the most surprising and potentially claims is that nonmagnetic semiconductors as Ge and GaAs become ferromagnetic by doping with a few percent of 3d transition metals (TM) as Mn [4-6]. One of the most important issues that need to be solved is how

to enhance their Curie temperature (T_c), which remains far below room temperature (RT). Diluted magnetic oxides (DMO) are wide bandgap oxides as SnO$_2$, TiO$_2$, ZnO, etc., that can be used as host semiconducting oxides, and doping with most of the 3d transition metals will produce RT ferromagnetism (FM) [7-9]. However, this is not always successful, as nonmagnetic materials can be obtained depending on the synthesis process and crystal characteristics [7-9]. Research on the physical mechanism governing the ferromagnetic order on DMOs has focused mainly on the following aspects: (a) oxygen vacancy (V$_O$) defects [10,11], (b) interstitial cations defects [12], and (c) 3d TM doping [13,14]. The concentration of the doping element remains below the percolation limit established by the relation $x_p \sim 2/Z_0$, where Z_0 is the coordination number of the cation [15], for SnO$_2$ $x_p \sim 32$ at.% [16], and this concentration is only limited by the solubility limit of the dopant. However, the concentration of dopant cations is chosen, in most of the cases, below 10 at.% to avoid antiferromagnetic (AFM) coupling between neighboring 3d cations. A particular

* Correspondence: sion.olive@cimav.edu.mx
[1]Centro de Investigación en Materiales Avanzados, S.C., Cimav, Av. Miguel de Cervantes 120, Complejo Industrial Chihuahua, C.P. 31109 Chihuahua, Chihuahua, Mexico
Full list of author information is available at the end of the article

feature observed on DMO thin films is that different saturation magnetizations (M_s) are obtained depending on the crystallographic direction on which the magnetic M (H) measurement is performed. In other words, M_s obtained in different crystallographic directions does not converge at large magnetic fields as conventional ferromagnetic films do [17]. Normally, in DMO out-of-plane $M_s^\perp$ is 2 to 3 times higher than in-plane $M_s^{//}$ [18,19], suggesting that spin-orbit interaction in these materials is very strong and that measured M_s is in fact the spin component along a given direction. Furthermore, M(H) loops in DMO are anhysteretic, and maximum values of coercivity reach some teens of oersted (Oe). Research on 3d TM-doped SnO_2 thin films was highly motivated after Ogale et al. [20], reported a giant magnetic moment of 7.5 μ_B/Co with a high T_C =650 K on 5 at.% Co-doped SnO_2 epitaxial thin films. In this paper, we present a detailed study of the evolution of the intensity of the magnetic moment per Co atom (either FM or AFM) on Co-doped SnO_2 thin films sputtered on SiO_2/Si(001) substrates at RT followed by thermal treatments in vacuum under magnetic field applied out-of-plane and in-plane configurations.

Methods

Thin films were elaborated using a sputtering system from Intercovamex (Intercovamex, Cuernavaca, Mor, Mexico), with a base pressure of 1×10^{-6} Torr. A home-made SnO_2 target with Co inclusions was prepared following conventional ceramic methods from high-purity SnO_2 and Co powder, both with 99% purity from Sigma-Aldrich (Sigma-Aldrich, St. Louis, MO, USA). In a first step, SnO_2 powders were milled in a high-energy mill 8000D SPEX (Spex Industries, Inc., Metuchen, NJ, USA), for 1 h with ethanol, and then, Co powder was added in stoichiometric proportion to obtain the formula $Sn_{0.95}Co_{0.05}O_2$. The mixture was dried at room temperature and compressed at 4.2 MPa followed by sintering at 1,200°C for 1 h. The obtained pellet had 1-in. diameter. Substrates were 2×2 cm^2 sections cut from an 8-in. diameter SiO_2/Si(001) wafer. Substrates were first cleaned by an ultrasonic bath for 10 min with ethanol, then rinsed with deionized water, and finally dried with synthetic air. Thin film deposition was achieved using a radio frequency (RF) source at 90 W for 30 min at RT. From a selected sample, four equal 5×5 mm^2 sections were cut in order to apply the thermal treatment (TT) with and without an applied magnetic field (H_{TT}). A vacuum tubular furnace [see Additional file 1] was constructed for this purpose and was placed between the poles of an electromagnet. A sample holder inside the furnace allows the placement of the sample parallel (PL) or perpendicular (PP) to the direction of H_{TT}. Annealing was performed at 600°C for 20 min, and the intensity of H_{TT} =0.73 T was
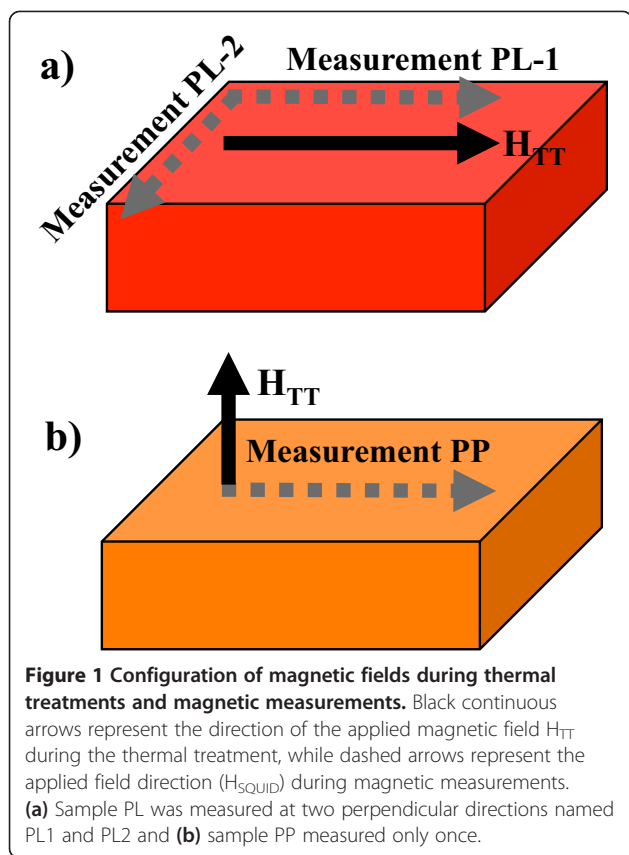
kept during heating and cooling processes. The samples were named as follows: sample PL, where H_{TT} was applied parallel to the sample surface; sample PP, where H_{TT} was applied perpendicular to the surface; sample NF (no-field) annealed without magnetic field; and as-grown sample is named sample AG. The structural characterization was carried out using grazing incidence X-ray diffractometry (GIXRD), with a fixed incident angle of 0.5° in a PANalytical X'Pert equipment (PANalytical, Lelyweg, Almelo, Holland, The Netherlands). Sample preparation for transmission electron microscopy (TEM) was carried out in a focused ion beam equipment from Jeol (Jeol, Sendai, Japan) and analyzed with a field emission TEM, a Jeol JEM 2200Fs + Cs (Jeol, Musashino, Akishima, Tokyo, Japan). The composition of the film at different points from the surface to the interface with the substrate was obtained by energy dispersive X-ray spectroscopy (EDS) using Oxford spectrometer and INCA software during TEM observations. Magnetic M(H) measurements were performed at 2 and 300 K with a maximum applied magnetic field of 6 T using a superconducting quantum interference device (SQUID) equipment from Quantum Design (SQUID, San Diego, California, USA). For sample PL, two in-plane magnetic measurements were performed: PL1, where the magnetic field from SQUID (H_{SQUID}) was applied parallel to the direction of H_{TT}; and PL2, where H_{SQUID} is perpendicular to H_{TT}. Measurements PL1 and PL2 are perpendicular to each other. Only one in-plane measurement was performed on sample PP, named measurement PP. A diagram depicting these measurements is shown on Figure 1.

Results and discussion

The GIXRD patterns obtained for all samples including the Co-doped SnO_2 target are shown on Figure 2a. All the peaks belong to the SnO_2-rutile structure, and no secondary phases as CoO, Co_3O_4, and stannic compounds or pure Co (for the target) were detected. GIXRD from sample AG shows a high substrate signal that covers the intensity of the SnO_2-rutile peaks; this is due to the random arrangement of the grains in the sample, before any TT. However, perfect randomness is not attained, and there is a trace of crystallinity represented by a small (101) peak, corresponding to the family of planes which is preferred for SnO_2-rutile thin films (called short-range order) [4], and it may be assumed that no texture is present. Besides, at RT is possible to adduce to the nucleation and crystal growth theory, where a relation between temperature and critical radius r^* for stable nuclei is given by:

$$r^* = \frac{2\sigma \cdot V}{kT \ln S} \qquad (1)$$

where σ is the surface-free energy, V is the theoretical volume of each atom in the crystal, k is the Boltzmann

Figure 1 Configuration of magnetic fields during thermal treatments and magnetic measurements. Black continuous arrows represent the direction of the applied magnetic field H_{TT} during the thermal treatment, while dashed arrows represent the applied field direction (H_{SQUID}) during magnetic measurements. **(a)** Sample PL was measured at two perpendicular directions named PL1 and PL2 and **(b)** sample PP measured only once.
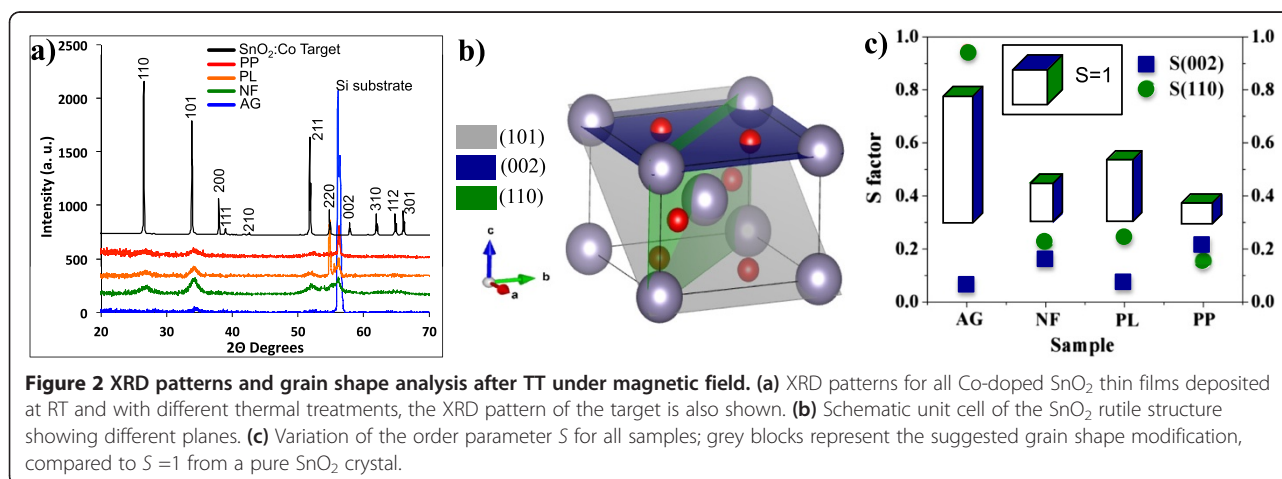
constant, T is absolute temperature, and S is the supersaturation ratio. At RT, there is a larger critical radius that must be reached before crystal growth is achieved. This radius decreases as temperature increases. At this point (higher temperatures), there is a high probability of forming stable nuclei from which grains start to grow. High substrate temperatures make possible the growth of thin films with better crystal quality than those grown at RT. Annealing at 600°C confers enough energy to disordered atoms to promote diffusion allowing crystal

rearrangement and crystal growth. In other words, annealing at 600°C induces a crystallization of the SnO$_2$-rutile phase. For sample PL, we observed the presence of a peak at 55.11°, corresponding to SnO$_2$(110) plane, suggesting an induced texture due to the direction of the magnetic field. This distribution of preferred orientations suggests that an increase in the number of (110) planes is favored by a strong perpendicular component of the spin direction of Co-doped SnO$_2$ grains, which may be assumed as the easy magnetization axis. Further structural analysis (not shown) by means of HR-TEM reveals a small increase on the grain size, due to the TT. We found an average grain size of 15 nm for sample AG that increases to 20 nm for sample PL. Analyzing the relative intensities of the peaks of the XRD patterns, the order parameter S [21,22] related to the grain shape, which is defined as:

$$S_{(hkl)C} = \sqrt{\frac{I_{(hkl)E}/I_{(h'k'l')E}}{I_{(hkl)T}/I_{(h'k'l')T}}} \qquad (2)$$

where $I_{(hkl)E°}$ and $I_{(h'k'l')T}$ correspond to experimental and theoretical intensities of a given plane, and $I_{(hkl)E}$ and $I_{(h'k'l')T}$ correspond to experimental and theoretical intensities for those families of lattice planes which show a particular change. This equation was used to establish the effect of H_{TT} on the morphology of the Co-doped SnO$_2$ grains in the film. A pure SnO$_2$ crystal has a specific shape in order to minimize the total surface-free energy corresponding to S order parameter equal to one, depicted on the inset of Figure 2c. The change on the intensity of certain peaks provides a number to describe morphological changes. Applying Equation 2 to the intensities of (002) and (110) peaks compared to the intensity of (101) peak, which is normally parallel to the substrate surface for SnO$_2$ thin films (Figure 2b), it is possible to calculate the order parameter S and determine the relative grain shape. This grain shape evolution is attributed to the growth along a component of the spin direction, which is

Figure 2 XRD patterns and grain shape analysis after TT under magnetic field. (a) XRD patterns for all Co-doped SnO$_2$ thin films deposited at RT and with different thermal treatments, the XRD pattern of the target is also shown. **(b)** Schematic unit cell of the SnO$_2$ rutile structure showing different planes. **(c)** Variation of the order parameter S for all samples; grey blocks represent the suggested grain shape modification, compared to S =1 from a pure SnO$_2$ crystal.

parallel to the direction of H_{TT} during TT. This assumption can explain how grain growth is favored along some defined directions by the direction of H_{TT}. In Figure 2c, the relative intensities of the S order parameter and a representation of the grain shape for each sample compared to that of pure SnO_2 grains are shown.

Figure 3 shows a TEM cross-sectional view of sample PL where the film thickness is ~300 nm. Punctual EDS analysis, indicated by red points in the figure, was performed during TEM observations in order to evaluate the atomic Co distribution on the film (i.e., x on the formula $Sn_{1-x}Co_xO_2$, at.% = $x \times 100$). Near to the interface with the substrate, Co concentration is x ~13 at.% that decreases as the probe moves towards the surface reaching a minimum value of ~2%. This reduction of Co concentration is attributed to an induced oxidation of the exposed Co particles on the target, during sputtering process, making them harder to erode. The high Co concentration near the interface has a significant effect on the magnetic properties, as it will be further described.

To evaluate the effect of H_{TT} on the magnetic properties of the films, magnetic M(H) measurements PL1, PL2, and PP were performed at 2 and 300 K. Figure 4a shows M(H) loops obtained at 2 K, depicting an apparent ferromagnetic and paramagnetic (inset) behavior. A first attempt to elucidate the magnetic behavior of the films was to fit the experimental loops with the Brillouin function, which describes the magnetization process for any FM or AFM material:

$$B\left(J, a'\right) = \frac{2J+1}{2J} \cot\left(\frac{2J+1}{2J}\right) \cdot a' - \frac{1}{2J} \coth\frac{a'}{2J} \quad (3)$$
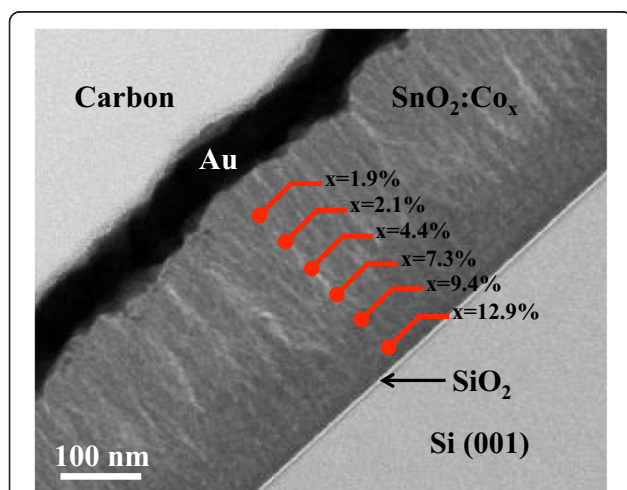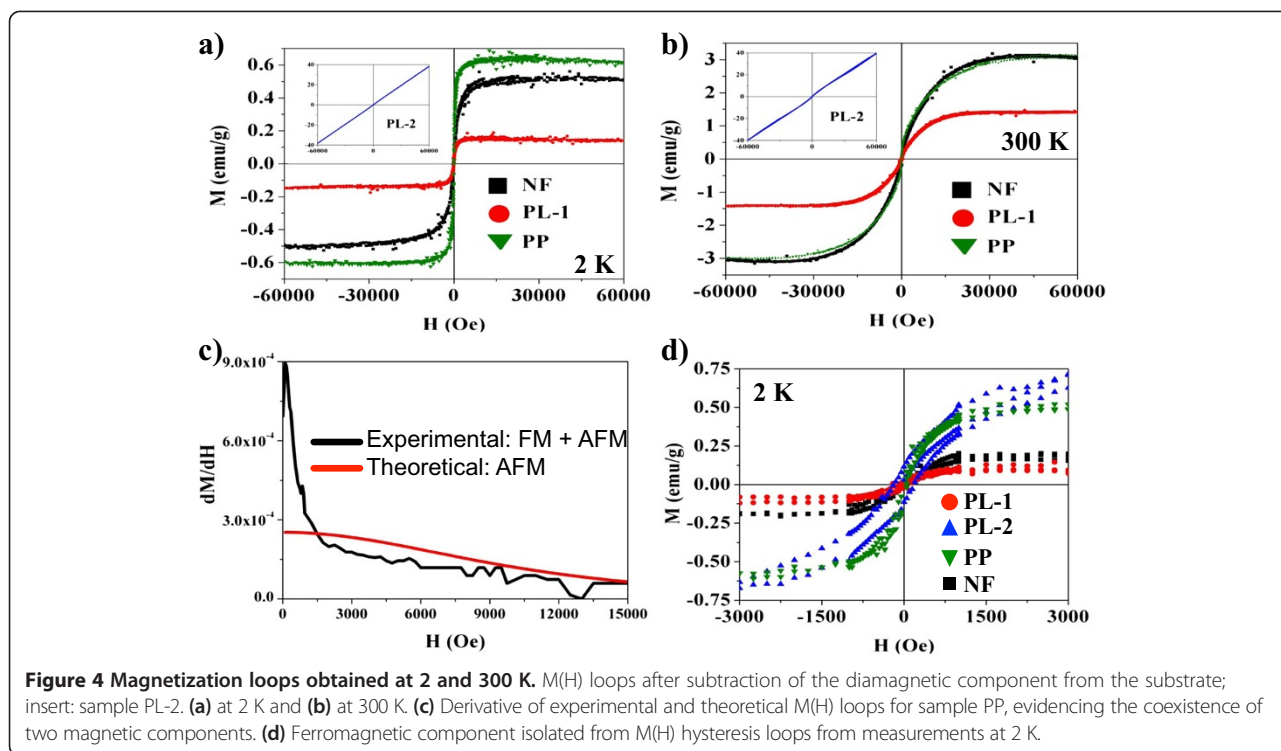

Figure 3 TEM and EDS analysis for sample PL. Cross-sectional view of sample PL showing the Co variation on atomic percent (indicated by x in the figure) at different points from the surface to the interface with the substrate. Carbon and Au layers are used as protection barrier and electrical ground for FIB preparation.

where $a' = \mu_H H / KT$, μ_H is the maximum magnetic moment of Co atoms on the field direction and $J = 1/2$ as only spin component appears. Quenching effect on 3d TM makes $L = 0$; $J = L + S$. However, a closer look at the origin of the M-H plane, leads to define two magnetic phases as an abrupt change on the slope has detected. To make evident in this fact, the derivative of the first quadrant, of both, the experimental and the fitted Brillouin curves, was obtained for all measurements. In Figure 4c, the results for sample PP are shown. The derivative of the experimental measurement decreases abruptly from 0 to 1,500 Oe, then it decreases softly with almost the same rate than that of the fitted curve, and this is the demonstration of the coexistence of two magnetic phases. To elucidate the nature of the two components, we focus on measurement PL2, which seems to be paramagnetic; however, paramagnetic susceptibility varies with temperature through the expression, $X = C/T$, where C is the Curie constant. PL2 measurements at 2 and 300 K have the same slope, and then, paramagnetic behavior is discarded. Furthermore, the solubility limit of Co on SnO_2 is 2 at.% [18] thus, near to the interface with the substrate where Co concentration is ~13 at.%, an AFM coupling is expected. Perpendicular AFM susceptibility ($X_\perp$) is not temperature dependent below Néel temperature (T_N). AFM coupling of Co atoms in the rutile structure may be similar to superexchange interaction on CoO where $T_N = 292$ K [23]. Equation 3 was used to evaluate the AFM magnetic moment (m) per Co atom, by fitting to the experimental measurements NF, PL1, and PP. The maximum AFM moment $m = 7.01$ μ_B/Co was obtained on sample PL. For measurement PL2, we used the equation for perpendicular anisotropy in an antiferromagnetic material:

$$X_\perp = \frac{C}{2\theta_P} \quad (4)$$

where θ_P is the paramagnetic Curie temperature (calculated from $1/X$ vs. T plot, insert Figure 5) and C the Curie constant $C = N\mu^2/3Ak$, where N is Avogadro number, μ is the magnetic moment per atom, and A is the atomic weight. The slope of the AFM component is equal to $X_\perp$ from where the AFM moment $m = 6.54$ μ_B/Co at. is obtained, which is similar to the one obtained on PL1 measurement (7.01 μ_B/Co). From this analysis, the direction of PL2 measurement corresponds to an induced spin axis of the AFM pairs, due to the effect of TT under H_{TT}. On sample PP, the AFM moment decreases to 4.96 μ_B/Co at. suggesting that AFM coupling is more stable when spin axis is oriented parallel to the substrate surface. It may be observed how AFM component almost vanishes at 300 K, which is a temperature barely lower than T_N in our samples. Using the intensity of the magnetic moments

Figure 4 Magnetization loops obtained at 2 and 300 K. M(H) loops after subtraction of the diamagnetic component from the substrate; insert: sample PL-2. **(a)** at 2 K and **(b)** at 300 K. **(c)** Derivative of experimental and theoretical M(H) loops for sample PP, evidencing the coexistence of two magnetic components. **(d)** Ferromagnetic component isolated from M(H) hysteresis loops from measurements at 2 K.

of each sample and the m per Co atom, we found that 46% of the total Co atoms are AFM coupled.

In a second step, to quantify the FM component per Co atom, the Brillouin fit was subtracted from the experimental measurements to obtain a FM loop as shown on Figure 4d. The total magnetic moment of the sample is divided by the remaining amount of FM Co atoms to obtain the individual m. In Table 1,

the m for all samples at 2 and 300 K is shown. The source of the FM component is attributed to the BMP model on DMO [24]. Magnetic moments from measurements PP and PL2 at 2 K are m =0.31 and 0.42 μ_B/Co at., which decreases to 0.018 and 0.12 at 300 K, respectively. The m of sample PP remains more stable against temperature perturbations demonstrating that the FM m has a strong component perpendicular to the substrate.

In Figure 5, the ZFC-FC measurement performed on sample PP is shown and the increasing magnetization with decreasing temperature has been observed in other DMO systems [25,26], similar to that of a superparamagnetic system with the difference that there is no any observed blocking temperature. The peak observed at 41 to 47 K can be attributed to a minority of Co_3O_4 precipitates undetectable by XRD experiments. The $1/X$ graph presented on the insert shows that the extrapolation of the straight dotted line intercepts the temperature axis at a negative value of T, corresponding to the paramagnetic Curie temperature θ_P.
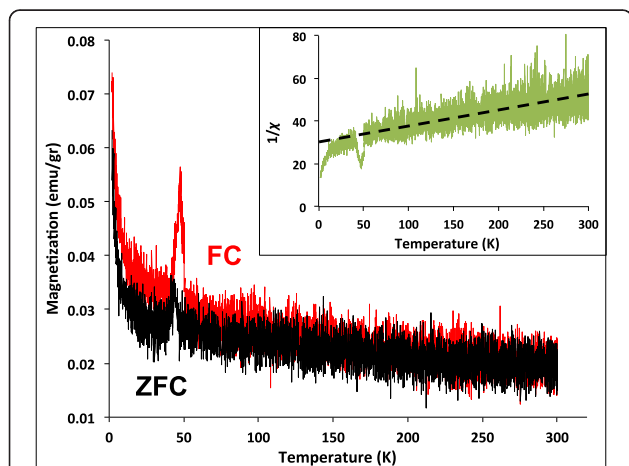

Figure 5 ZFC-FC performed on sample PP. Typical ZFC-FC curves observed on DMO system, and the peak at 41 to 47 K is attributed to a minority Co_3O_4 AFM nanoclusters. In the inset, an extrapolation of the $1/X$ curve intercepts the temperature axis at a negative value demonstrating that a part of Co atoms is AFM coupled.

Table 1 Magnetic moments m in μ_B per Co at. obtained from all measurements at 2 and 300 K

Measurement		NF	PL-1	PL-2	PP
AFM moment	2 K	5.39	7.0119	6.5466	4.96
FM moment	2 K	0.0629	0.0642	0.3125	0.4285
	300 K	0.0320	0.0178	0.0180	0.1216

Crystal field theory (CFT) was used to explain these results in agreement with the anisotropy feature in DMO thin films. For schematic purposes, in Figure 6, a Co^{2+} ion is placed at the center of the octahedron formed by O atoms on the rutile cell. The 3d orbitals of the Co atom according with the CFT are dz^2 and dx^2-y^2, which are degenerated, in a higher energy level than orbitals d_{xy}, d_{xz}, and d_{zx}. Mimaki et al. [27] studied the bond character of rutile type on SiO_2, GeO_2, and SnO_2, and they observed that the ratio of the electron density of M-O equatorial distances/M-O axial distances (where M is Si, Ge, or Sn) decreases when increases the atomic number of the cation. Then, for SnO_2, the electron density is higher on the dz^2 orbital and only one unpaired electron will be occupying in this orbital. The FM moments per Co at. are very small, suggesting that the Co atoms have a low spin configuration. This fact is in agreement with the measurements that a higher magnetic moment was obtained for sample PP, this is because dz^2 orbital axis forms an angle of 34.1° with SnO_2(101) plane (which remains parallel to the surface), and we assume a very strong spin - orbit coupling. With the TT applied in the PP configuration, the vertical component of the spin is aligned in the same direction than that of the magnetic field. The contribution of the possible random orientations of the SnO_2 cells is represented in Figure 6a. For PL configuration, the alignment of the spins is in a manner that the horizontal components are parallel to the applied field of the TT, as shown in Figure 6b, and the addition of all these components leads to a total magnetic moment lower than

that of the PP configuration. These results can be compared with monocrystalline thin films (e.g., epitaxial films on r-cut sapphire substrate), where the spin components can be better appreciated, and different magnetizations are obtained for PL and PP configurations.

Conclusions

Polycrystalline Co-doped SnO_2 thin films were grown by RF sputtering at room temperature. Crystallinity of the films was improved by thermal treatment at 600°C with and without an external magnetic field. The relative intensities of (002) and (110) peaks of the XRD patterns were compared with the intensity of the (101) peak, through the order parameter S related to the shape of the nanocrystals. The thermal treatment under magnetic field changed the shape of the crystals, as growth is favored along the direction where the spin is aligned. The analysis of magnetic properties resulted in the observation of two magnetic phases: ferromagnetic (FM) and anti-ferromagnetic (AFM), where AFM component has a Néel temperature barely higher than RT arising from the coupling between Co atoms in the region near to the interface with the substrate, where Co concentration is ≈ 13 at.%, which is higher than the solubility limit of Co on SnO_2. Moreover, a modification of crystal anisotropy due to the thermal treatment under magnetic field was observed, enhancing the FM moment for films where the magnetic field during thermal treatment was applied in a direction perpendicular to the substrate surface. The FM moment produced by Co ions arises from the interaction of these ions through the spherical orbit of the electron

Figure 6 Proposed model indicating the location and orientation of the spin on the orbital dz². Red continuous arrows represent the location and orientation of the spin, and black dashed arrows represent the spin components considered in the obtained FM moments. Red dashed arrows give a qualitative indication of the magnitude of the ferromagnetic moment obtained for each studied case. **(a)** For sample PP, as the spin-orbit interaction is very strong, the vertical component of the spin will align with the applied magnetic field during the TT. **(b)** For sample PL, the horizontal component will align with the direction of the field during TT and the total component is smaller than that of **(a)**.

on the polaron produced by the oxygen vacancy. As the intensity of the magnetization depends on the direction in which the measurement is done and as dz^2 orbital has the highest probability to contain the unpaired electron, then, we suggest that the spin is perpendicular to the axis of this orbital and parallel to the [101] direction. Proposing that this direction $[101]_{SnO2}$ is the easy axis of magnetization and that magnetization measured along any direction corresponds to the spin component.

Additional file

Additional file 1: Tubular furnace. Schema showing the tubular furnace used for the TT under magnetic field (H_{TT}). The sample is placed at the interior of the tubular ceramic element parallel or perpendicular to the direction of H_{TT}.

Competing interests
The authors declare that they have no competing interests.

Authors' contributions
SMLM participated in the thin films growth, data collection, and interpretation. She also worked on the manuscript. PP and RD gave the facilities and performed the magnetic measurements. HEEP participated in the thin films growth and gave equipment facilities. ILTO constructed the vacuum tubular furnace for thermal treatments. OOSC participated in the thin films preparation for TEM analysis and equipment facilities. CEOG performed TEM observation and EDS analysis. FEM participated on the manuscript and SFOM participated in the thin films growth, the data interpretation, and the work on the manuscript. All authors read and approved the final manuscript.

Authors' information
SMLM is a Ph.D. student in materials sciences at CIMAV. PP is a senior researcher at the National Chemical Laboratory (NCL) in India, and RD is a Ph.D. student at NCL. The rest of the authors work at Cimav Chihuahua. ILTO works as a technical engineer for general laboratory support. OOSC is in charged for the TEM sample preparations using FIB. CEOG performs the TEM observations. FEM is a professor researcher working with the theoretical calculations, and HEEP is a researcher working on the thin films by sputtering. SFOM is a experimental researcher and head of the group.

Author details
[1]Centro de Investigación en Materiales Avanzados, S.C., Cimav, Av. Miguel de Cervantes 120, Complejo Industrial Chihuahua, C.P. 31109 Chihuahua, Chihuahua, Mexico. [2]Physical and Materials Chemistry Division, National Chemical Laboratory, Dr. Homi Bhabha Road, Pune 411008, India.

References
1. Ali M, Tuna S, Fedakar E, Aytunç A: **Synthesis, characterization and dielectric properties of SnO$_2$ thin films.** *Spectrochim Acta Part A* 2014, **133**:60–65.
2. Padilla D, Vadillo JM, Laserma JJ: **Room temperature pulsed laser deposited ZnO thin films as photoluminescence gas sensors.** *Appl Surf Sci* 2012, **259**:806–810.
3. Kumar Y, Escorcia J, Singh F, Olive SF, Sivakumar VV, Kanjilal D, Agarwal V: **Influence of mesoporous substrate morphology on the structural, optical and electrical properties of RF sputtered ZnO layer deposited over porous silicon nanostructure.** *Appl Surf Sci* 2012, **258**:2283–2288.
4. Spiesser A, Sato Y, Saito H, Yuasa S, Ando K: **Epitaxial growth of ferromagnetic semiconductor Ga$_{1-x}$Mn$_x$As film on Ge (001) substrate.** *Thin Solid Films* 2013, **536**:323–326.
5. Ma X, Lou C: **The ferromagnetic properties of Ge magnetic quantum dots doped with Mn.** *Appl Surf Sci* 2012, **258**(7):2906–2909.
6. Nazmul AM, Kobayashi S, Sugahara S, Tanaka M: **Control of ferromagnetism in Mn delta-doped GaAs-based semiconductor heterostrutures.** *Physica E* 2004, **21**(2–4):937–942.
7. Wu W, He Q, Jiang C: **Magnetic iron oxide nanoparticles: synthesis and surface functionalization strategies.** *Nanoscale Res Lett* 2008, **3**:397–415.
8. Goering E, Brück S, Tietze T, Jakob G, Gacic M, Adrian H: **Absence of element specific ferromagnetism in Co doped ZnO investigated by soft X-ray resonant reflectivity.** *J Phys Conf* 2010, **200**:092007.
9. Dogra R, Cordeiro MR, Carbonari AW, Saxena RN, Costa MS: **Absence of room temperature ferromagnetism in transition metal doped ZnO nanocrystalline powders from PAC spectroscopy.** *Hyperfine Interact* 2010, **197**:77–81.
10. Wang H, Yan Y, Mohammed YS, Du X, Li K, Jin H: **The role of Co impurities and oxygen vacancies in the ferromagnetism of Co-doped SnO$_2$: GGA and GGA + U studies.** *J Magn Magn Mater* 2009, **321**:3114–3119.
11. Zhao S, Bai Y, Chen J, Bai A, Gao W: **Optical and magnetic properties of copper doped zinc oxide nanofilms.** *J Magn* 2014, **19**:68.
12. Olive SF, Santillan CR, Gonzalez RA, Espinosa F, Matutes JA: **Role of vanadium ions, oxygen vacancies, and interstitial zinc in room temperature ferromagnetism on ZnO-V$_2$O$_5$ nanoparticles.** *Nanoscale Res Lett* 2014, **9**:169.
13. Vijayaprasath G, Murugan R, Ravi G, Mahalingam T, Hayakawa Y: **Characterization of dilute magnetic semiconducting transition metal doped ZnO thin films by sol-gel spin coating method.** *Appl Surf Sci* 2014. In Press, accepted manuscript.
14. Zhao S, Yao C, Lu Q, Song F, Wan J, Wang G: **Cluster-assembled cobalt doped ZnO nanostructured film prepared by low energy cluster beam deposition.** *Trans Nonferrous Met Soc Chin* 2009, **19**:1450.
15. Deutscher G, Zallen R, Adler J: *Percolation Structures and Processes.* Bristol: Adam Hilger; 1983.
16. Coey JMD: **Magnetism of dilute oxides. Handbook of spin transport and magnetism.** *Igor Žutić. Chapman and Hall/CRC* 2011, 405–425. 1st Ed.
17. Cullity BD, Graham CD: **Introduction to magnetic materials.** *Wiley-IEEE Press* 2009, 505–515. 2nd Ed.
18. Fitzgerald CB, Venkatesan M, Douvalis AP, Huber S, Coey JMD, Bakas T: **SnO$_2$ doped with Mn, Fe or Co: room temperature in dilute magnetic semiconductors.** *J Appl Phys* 2004, **95**:7390–7392.
19. Coey JMD, Venkatesan M, Fitzgerald CB, Dorneles LS, Stamenov P, Lunney JG: **Anisotropy of the magnetization of a dilute magnetic oxide.** *J Magn Magn Mater* 2005, **290–291**:1405–1407.
20. Ogale SB, Choudhary RJ, Buban JP, Lofland SE, Shinde SR, Kale SN, Kulkarni VN, Higgins J, Lanci C, Simpson JR, Browning ND, Das Sarma S, Drew HD, Greene RL, Venkatesan T: **High temperature with a giant magnetic moment in transparent Co-doped SnO$_{2-\delta}$.** *Phys Rev Lett* 2003, **91**(7):077025.
21. Steinhardt P, Nelson D, Ronchetti M: **Bond-orientational order in liquids and glasses.** *Phys Rev B* 1983, **28**:784.
22. Kurt H, Rode K, Venkatesan M, Stamenov P, Coey J: **High spin polarization in epitaxial films of ferrimagnetic Mn$_3$Ga.** *Phys Rev B* 2011, **83**:020405.
23. Voges F, De Gronckel H, Osthöver C, Schreiber R, Grünberg P: **Spin valves with CoO as an exchange bias layer.** *J Magn Magn Mater* 1998, **190**(3):183–186.
24. Coey JMD, Venkatesan M, Fitzgerald CB: **Donor impurity band exchange in dilute ferromagnetic oxides.** *Nature Mater* 2005, **4**:173–179.
25. Weibing C, Jingbo L: **Magnetic and electronic structure properties of Co-doped SnO$_2$ nanoparticles synthesized by the sol-gel-hydrothermal technique.** *J Appl Phys* 2011, **109**:083930.
26. Sati P, Hayn R, Kuzian R, Régnier S, Schäfer S, Stepanov A, Morhain C, Deparis C, Laügt M, Goiran M, Golacki Z: **Magnetic anisotropy of Co2+ as signature of intrinsic ferromagnetism in ZnO:Co.** *Phys Rev Lett* 2006, **96**:017203.
27. Mimaki J, Tsuchiya T, Yamanaka T: **The bond character of rutile type SiO$_2$, GeO$_2$ and SnO$_2$ investigated by molecular orbital calculation.** *Z Kristallogr* 2000, **215**:414–423.